# Surface diffusion in glasses of rod-like molecules posaconazole and itraconazole:

# Effect of interfacial molecular alignment and bulk penetration

- 3 Yuhui Li<sup>1</sup>, Wei Zhang<sup>1,3</sup>, Camille Bishop<sup>2</sup>, Chengbin Huang<sup>1</sup>, M. D. Ediger<sup>2</sup>, Lian Yu<sup>1\*</sup>
- <sup>1</sup> School of Pharmacy, University of Wisconsin-Madison, Madison, WI, 53705, USA
- <sup>5</sup> Department of Chemistry, University of Wisconsin-Madison, Madison, WI, 53706, USA
- 6 <sup>3</sup> Current Address: Genentech Inc., South San Francisco, CA, 94080, USA

**Abstract.** The method of surface grating decay has been used to measure surface diffusion in the glasses of two rod-like molecules posaconazole (POS) and itraconazole (ITZ). While structurally similar antifungal medicines, ITZ forms liquid-crystalline phases while POS does not. Surface diffusion in these systems is significantly slower than in the glasses of quasi-spherical molecules of similar volume when compared at the glass transition temperature  $T_{\rm g}$ . Between the two systems, ITZ has slower surface diffusion. These results are explained on the basis of the near-vertical orientation of the rod-like molecules at the surface and their deep penetration into the bulk where mobility is low. For molecular glasses without extensive hydrogen bonds, we find that the surface diffusion coefficient at  $T_{\rm g}$  decreases smoothly with the penetration depth of surface molecules and the trend has the double-exponential form for the surface mobility gradient observed in simulations. This supports the view that these molecular glasses have a similar mobility vs depth profile and their different surface diffusion rates arise simply from the different depths at which molecules are anchored. Our results also provide support for a previously observed correlation between the rate of surface diffusion and the fragility of the bulk liquid.

**Keywords**. Glass, surface diffusion, posaconazole, itraconazole, rod-like molecule, liquid crystal, mobility gradient.

#### Introduction

Surface mobility plays an important role in the physical stability of molecular glasses. Surface molecules can diffuse much faster than bulk molecules, <sup>1,2,3</sup> and this has been attributed to reduced local caging effect and smaller elastic penalty for rearrangement. <sup>4,5</sup> Surface mobility enables fast crystal growth in molecular glasses, reducing the shelf life of amorphous drugs <sup>6,7</sup> and motivating coating technologies for stabilization. <sup>8</sup> Surface mobility allows preparation of "ultra-stable glasses" by physical vapor deposition, taking advantage of the fast equilibration of just-deposited molecules before they are firmly embedded in the bulk. <sup>9,10</sup>

Surface diffusion can be measured by observing the evolution of surface contours driven by surface tension. 1,2,11,12,13,14 Previous work in this area has focused on molecular glasses containing quasi-spherical

molecules or slightly elongated molecules.<sup>3</sup> Motivated by recent attention to highly anisotropic glasses prepared with non-spherical molecules, <sup>15</sup> we have studied surface diffusion in the glasses of two rod-like molecules, posaconazole (POS) and itraconazole (ITZ) (see Scheme 1), both antifungal drugs. <sup>16,17</sup> While having similar structures, the two molecules differ in that ITZ forms liquid crystals (LC), <sup>18</sup> while POS does not. <sup>19</sup> This provides an opportunity to study the effect of bulk LC structure on surface diffusion. We find that surface diffusion is significantly slower in the glasses of POS

and ITZ than in the glasses of quasi-spherical molecules of similar

CI ON N-N Itraconazole (ITZ)

**Scheme 1.** Molecular structures of posaconazole (POS) and itraconazole (ITZ).

volume. This is attributed to the near-vertical orientation of the rod-like molecules at the surface and their deeper penetration into the bulk where mobility is low. Between the two systems studied, ITZ has slower surface diffusion, likely a result of the deeper penetration of surface molecules in this system.

Apart from investigating new types of molecules, this work was motivated by developing capabilities to predict surface diffusion rates. Chen et al. have analyzed all published surface diffusion results on molecular glasses and noted that the surface diffusion coefficient decreases smoothly with molecular size for van der Waals systems (no extensive hydrogen bonds).<sup>3</sup> They attributed this to a steep and generic mobility gradient beneath the surface of a molecular glass. Larger molecules insert themselves deeper into the bulk where mobility is lower, slowing down their center-of-mass diffusion. In this work we extend

their investigation to even deeper bulk penetration using the rod-like molecules and observe a greater retardation of diffusion. Our results uphold the previous conclusion and our mobility vs depth profile displays the double-exponential form characteristic of surface mobility gradient seen in simulations.<sup>20,21</sup> This finding is useful for predicting surface diffusion from molecular structures. We also examine a previously observed correlation between the rate of surface diffusion and the fragility of the bulk liquid.

**Experimental Section** 

Posaconazole (POS, purity > 98%) was obtained from Biochempartner and itraconazole (ITZ, purity > 99%) from Alfa Aesar. The materials were used as received. To make a surface grating, a master pattern was placed on a viscous liquid of POS or ITZ at 363 K and was peeled off after vitrifying the liquid at 298 K. This yielded a glass film with a sinusoidal surface contour. Master gratings of different wavelengths were obtained as follows: for  $\lambda = 1000$  nm and 1984 nm, plastic gratings purchased from Rainbow Symphony were used; for  $\lambda = 334$  nm, the masters were duplicated from a Blue-ray disc through a UV-curing polymer (Norland Optical Adhesive 61); for  $\lambda = 553$  nm, the masters were duplicated from a glass grating (Spectrum Scientific) through the same polymer. All masters were coated with 10 nm gold before use (Sputter deposition system, Leica ACE600). The thickness of each embossed glass film was 50 - 100 µm, much larger than the wavelength of any surface grating used, ensuring that the evolution of the top surface was unaffected by the substrate.

The flattening of a surface grating over time was monitored by Atomic Force Microscopy (AFM, Bruker Veeco Multiple Mode IV) or laser diffraction. AFM was performed in the tapping mode at room temperature; the height profile was Fourier transformed to obtain the amplitude of the sinusoidal surface. Laser diffraction was measured in transmission and used to determine faster decay than feasible with AFM. A HeNe laser ( $\lambda$  = 632.8 nm, Uniphase Corp.) passed through a sample film perpendicularly and the first-order diffraction in transmission was recorded with a silicon amplified detector (Thorlabs) interfacing with a National Instruments LabVIEW program. The grating amplitude was verified to be proportional to the square root of diffraction intensity. The diffraction method was used only for POS since the cloudiness of LC phases made transmission experiments difficult for ITZ. The two methods yielded identical results within experimental error when applied to the same decay process. During grating decay, the sample was

purged with dry nitrogen and its temperature was controlled within 0.1 K with a Linkam microscope temperature stage or a custom-made mini-oven.

## **Mullins' Theory of Surface Evolution**

According to Mullins,  $^{22}$  the amplitude h of a sinusoidal surface contour decreases exponentially over time,

 $h = h_0 \exp(-Kt)$ , and the decay rate *K* is given by:

93 
$$K = Fq + Aq^2 + (A' + C)q^3 + Bq^4$$
 (1)

94 where

95 
$$q = 2\pi/\lambda$$

$$F = \frac{\gamma}{2\eta}$$

97 
$$A = \frac{p_0 \gamma \Omega^2}{(2\pi m)^{1/2} (kT)^{3/2}}$$

$$A' = \frac{\rho_0 D_G \gamma \Omega^2}{kT}$$

$$C = \frac{D_v \gamma \Omega}{kT}$$

$$B = \frac{D_s \gamma \Omega^2 \nu}{kT}$$

In eq. (1),  $\lambda$  is the grating wavelength,  $\gamma$  is the surface tension,  $\eta$  the viscosity,  $p_0$  the vapor pressure at equilibrated state,  $\Omega$  the molecular volume, m the molecular weight,  $\rho_0$  the vapor density at equilibrated state,  $D_G$  the diffusion coefficient of the vapor molecules in an inert atmosphere,  $D_v$  the self-diffusion coefficient in the bulk,  $\nu$  the areal density of molecules on the surface, and  $D_s$  the surface diffusion coefficient. The different terms in eq. (1) correspond to different mechanisms of surface evolution: viscous flow (the F term), evaporation-condensation (A and A'), bulk diffusion (C), and surface diffusion (B). For each decay mechanism, the decay rate has a characteristic dependence on the grating wavelength, useful for identifying the mechanism; for example,  $K \propto \lambda^{-1}$  for viscous flow and  $K \propto \lambda^{-4}$  for surface diffusion. Mullins' method has been applied to measure the surface diffusion of many materials, both crystalline<sup>23</sup>

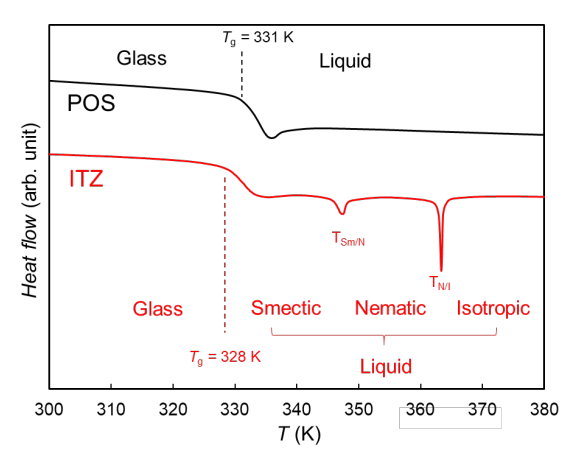
and amorphous.<sup>1,3</sup> In the case of a glass-forming Lennard-Jones liquid, Malshe et al. showed by simulations that the surface diffusion constant determined by Mullins' method agrees with that calculated from the mean squared displacement of particles.<sup>24</sup>

# 

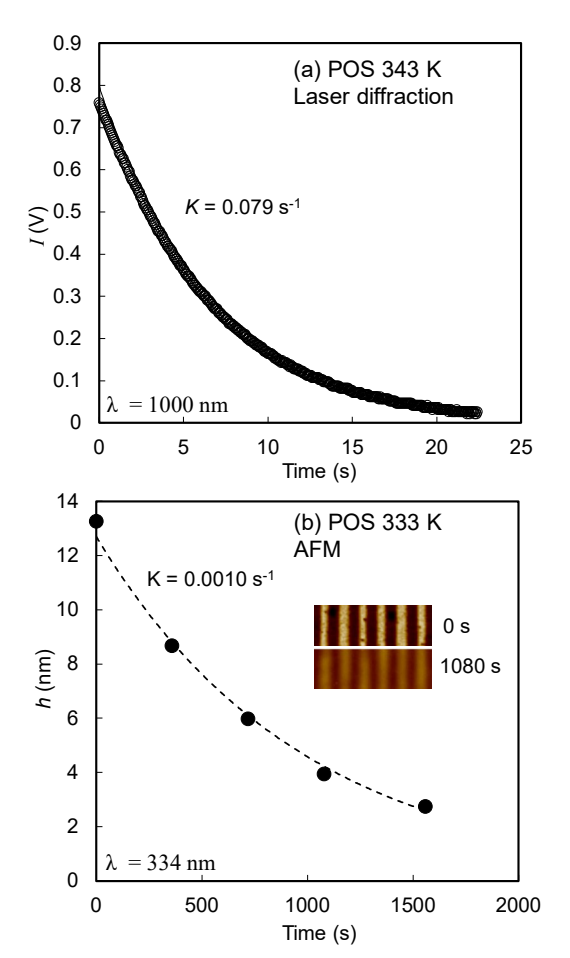
# Results

Figure 1 shows the DSC traces of POS and ITZ. The two liquids have similar  $T_g$ s with the value for ITZ being slightly lower. The lower  $T_g$  of ITZ is consistent with the dielectric spectroscopy results, <sup>18,19</sup> which show that ITZ has a shorter structural relaxation time at the same temperature. Different from POS, ITZ undergoes two phase transitions in the liquid state. <sup>18</sup> Cooling from a high temperature, an isotropic liquid of ITZ transforms into a nematic phase ( $T_{N/I}$ = 363 K) and then to a smectic phase ( $T_{Sm/N}$ = 347 K).

**Posaconazole (POS).** Figure 2 shows the typical decay kinetics of a POS surface grating recorded by laser diffraction (Figure 2a) and by AFM (Figure 2b). In each case, the decay was exponential, consistent with Mullins' theory.<sup>22</sup> The data were fit to the function  $\phi = exp(-Kt)$ , where  $\phi$  is  $h/h_0$  for AFM measurements and  $(I/I_0)^{1/2}$  for diffraction measurements and K is the decay constant.



**Figure 1.** DSC traces of POS and ITZ during heating at 10 K/min. Both systems show a glass transition ( $T_g$ ) and ITZ shows two LC transitions.



**Figure 2.** Typical decay kinetics of POS surface gratings. (a) At 343 K, recorded by laser diffraction ( $\lambda$  = 1000 nm). I is the diffraction intensity. (b) At 333 K recorded by AFM ( $\lambda$  = 334 nm). Inset: AFM images at two time points.

Figure 3a shows the decay constant K of POS at  $\lambda = 334$ nm as a function of temperature. The structural relaxation time of the POS liquid<sup>18</sup> is also shown for comparison; for this plot, we have extrapolated the experimental data below 331 K using the Vogel-Fulcher-Tammann (VFT) equation. At high temperatures, K closely tracks the structural relaxation time,  $K \propto \tau_{\alpha}^{-1}$ . Given that viscosity is generally proportional to  $\tau_{\alpha}$ , this indicates that viscous flow is the mechanism of surface flattening (the F term in eq. (1)). For this mechanism, the decay rate should be inversely proportional to the surface grating wavelength,  $K \propto \lambda^{-1}$ , and this was found to be the case (Figure 3b, see the 338 K result). This relation has been used to convert the *K* values measured at longer wavelengths to the values at  $\lambda = 334$  nm so they can be included in Figure 3a to extend the measurement to higher temperatures.

138

139

140

141

142

143

144

145

146

147

148

149

150

151

152

153

154

155

156

157

158

159

160

161

162

163

164

165

166

167

Although viscous flow accounts for the decay rates observed at high temperatures, it does not at low temperatures (Figure 3a). The observed decay rate is "too fast" relative to viscous relaxation below 333 K ( $T_g + 2$ 

mechanism. (b) Wavelength dependence of K at two temperatures indicating decay by viscous flow at high temperatures and by surface diffusion at low temperatures. K). This suggests a change of mechanism for surface evolution, as observed in other systems. Figure 3b shows that in this lower temperature region, K has a stronger dependence on the surface grating wavelength,  $K \propto \lambda^{-4}$ , which is expected for the surface diffusion mechanism. Thus, we assign the mechanism of surface evolution to surface diffusion at low temperatures and use the observed decay rates to calculate the surface diffusion coefficients D<sub>s</sub> (Figure 4). For this calculation, we assume y = 0.05 N/m, a typical value for organic liquids, and obtain  $\Omega = 0.92$  nm<sup>3</sup>

-6

-7 -8

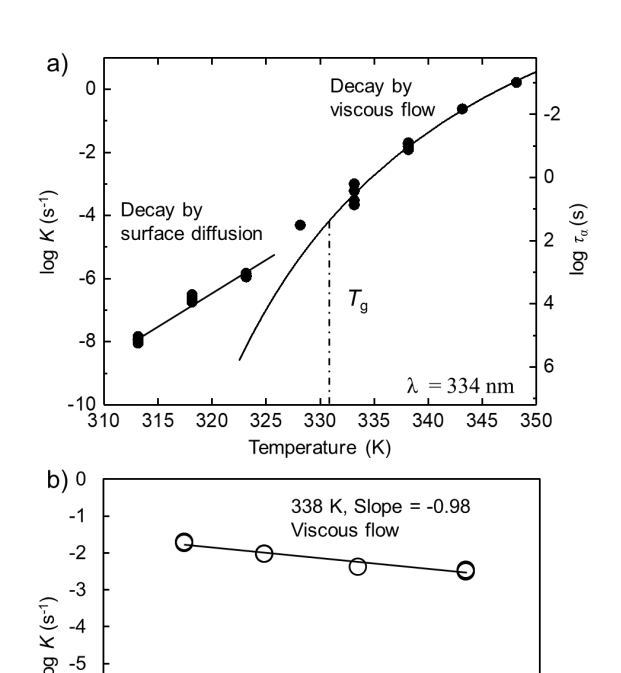
(molecular volume) from the density of a POS glass (1.27 g/cm<sup>3</sup>, assumed to be the same as that an ITZ

glass<sup>25</sup>) and its molecular weight (700.8 g/mol). For this rod-like molecule, we estimate its areal density

at the liquid/vapor interface by taking into account its preferred orientation. Bishop et al. used NEXAFS

2.3

2.5



 $\log \lambda (nm)$ Figure 3. (a) Decay constant K of a POS surface grating at  $\lambda$  = 334 nm as a function of temperature. At high temperatures, K tracks the structural relaxation time  $\tau_{\alpha}$  (second y axis) viscous flow controls surface indicating evolution. Decay becomes faster below  $T_g$  + 2 K, indicating a change of surface flattening

2.9

323 K, Slope = -4.1

Surface diffusion

3.1

3.3

3.5

to show that POS molecules are nearly vertical at the liquid/vapor interface.<sup>26</sup> Thus we estimate the areal density using:  $v \approx L/\Omega = 2.8 \text{ nm}^{-2}$ , where L is the length of a POS molecule (2.6 nm, taken from its crystal structure).<sup>27</sup> If POS is treated as a spherical molecule at the surface as opposed to an oriented rod, we obtain  $v \approx \Omega^{-2/3} = 1.0 \text{ nm}^{-2}$  and the calculated  $D_s$  would be larger by a factor of 3; given the 5 order of magnitude spread of surface diffusion coefficients (Figure 4), this is a relatively small effect.

Figure 4 compares the surface diffusion coefficient  $D_s$  of POS and other molecular glasses: ortho-terphenyl (OTP), <sup>28</sup> tris-naphthyl benzene (TNB), <sup>29</sup> griseofulvin (GSF), <sup>30</sup> indomethacin (IMC), <sup>1</sup> and polystyrene (PS) oligomers (1110 and 1700 g/mole). 31 Figure 4 also shows the bulk diffusion coefficients  $D_v$  of the same systems when available. 32,33,34,35 After scaling the temperature by  $T_{\rm g}$ , the  $D_{\rm v}$  values cluster to a "master curve". Relative to this, the  $D_s$  values are all larger and do not collapse into a single curve. Note that of all the systems studied to date, POS has the slowest surface diffusion in this comparison: its  $D_s$  at  $T_g$ , ~10<sup>-17</sup> m<sup>2</sup>/s (estimated by extrapolation), is 5 

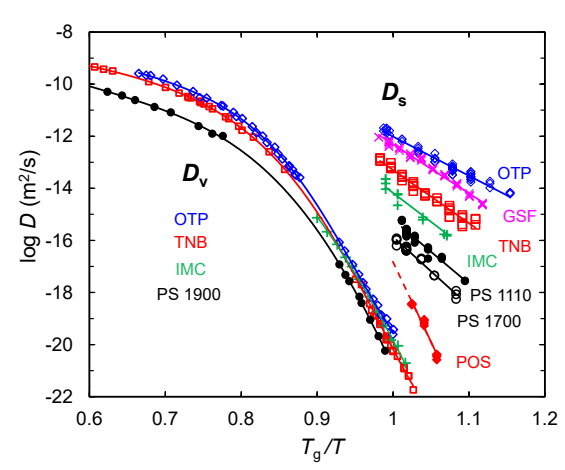


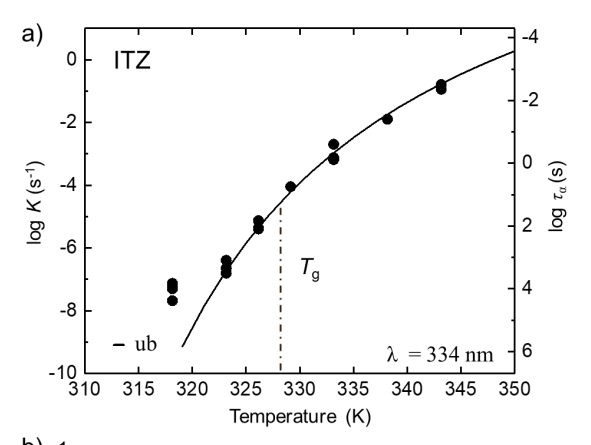
**Figure 4.** Surface diffusivity in POS and other molecular glasses.  $T_{\rm g}$  is the onset temperature measured by DSC during heating at 10 K/min after cooling at the same rate.

orders of magnitude smaller than the value for OTP. In addition, the  $D_s$  of POS has the strongest temperature dependence, with an activation energy (389 kJ/mol) close to that for bulk diffusion. The slow surface diffusion of POS will be discussed later and attributed to the near-vertical orientation of the surface molecules and their deep penetration into the bulk.

Itraconazole (ITZ). Figure 5a shows the surface-grating decay constant K of ITZ at  $\lambda = 334$  nm as a function of temperature. The bulk structural relaxation time<sup>18</sup> is also shown for comparison. As in the case of POS, the relation  $K \propto \tau_{\alpha}^{-1}$  is observed at high temperatures, indicating surface evolution by viscous flow. This is confirmed by wavelength tests (Figure 5b). At both 323 K and 333 K, we observe the relation  $K \propto \lambda^{-1}$ , as expected for the viscous-flow mechanism.

The key difference between ITZ and POS is that in ITZ, viscous flow controls surface evolution down to a lower temperature relative to  $T_{\rm g}$ . In ITZ, K tracks  $\tau_{\alpha}$  down to  $T_{\rm g}-5$  K (Figure 5a), whereas in POS, this is the case only down to  $T_{\rm g}+2$  K (Figure 3a), below which surface diffusion is fast enough to be the decay mechanism (Figure 3b). Thus, surface diffusion in ITZ must be slower than that in POS at the same temperature relative to  $T_{\rm g}$ .

To see the point above more clearly, in Figure 6, we plot the decay constant K against the bulk relaxation time  $\tau_{\alpha}$  for both systems. This allows a comparison of the two surface processes at the same bulk mobility. At high temperatures (short  $\tau_{\alpha}$ ), we find  $K \propto \tau_{\alpha}^{-1}$ , confirming surface evolution by viscous flow. In this region, the two systems have very similar decay rates at a common  $\tau_{\alpha}$  (bulk mobility), as expected for this mechanism. At low temperatures (long  $\tau_{\alpha}$ ), the observed decay is faster



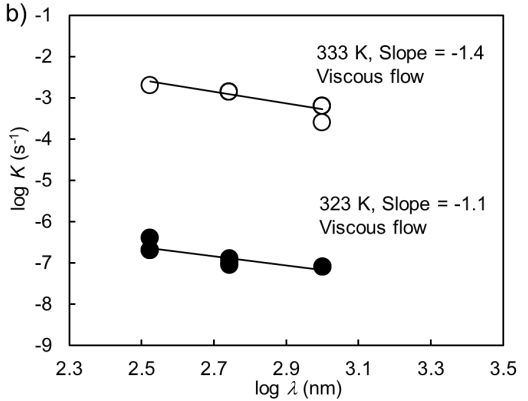


**Figure 5.** (a) Surface grating decay rate K of ITZ at  $\lambda$  = 334 nm as a function of temperature. "ub" indicates an upper bound from no significant decay in 250 days. (b) K as a function of grating wavelength  $\lambda$  at 323 K and 333 K.

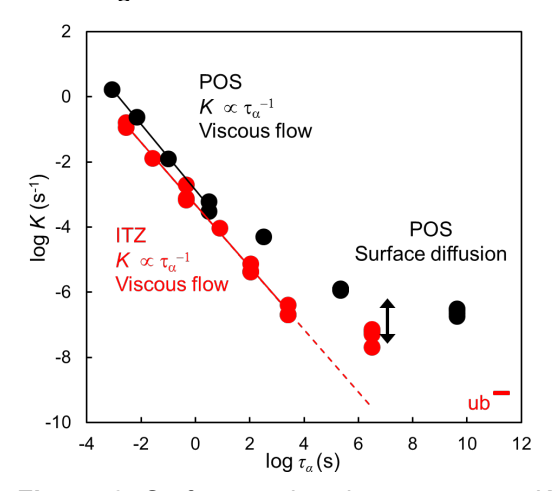


**Figure 6.** Surface-grating decay constant K at  $\lambda=334$  nm plotted against the bulk relaxation time  $\tau_{\alpha}$  for ITZ and POS. At high temperatures (short  $\tau_{\alpha}$ ),  $K \propto \tau_{\alpha}^{-1}$  holds, indicating surface evolution by viscous flow. At low temperatures (long  $\tau_{\alpha}$ ), faster decay is observed signaling a new decay mechanism.

relative to viscous flow, suggesting a change of decay mechanism. For POS, the new decay mechanism was shown to be surface diffusion by a wavelength test (Figure 3b). It is likely that the ITZ undergoes the same transition to surface diffusion at the lowest temperature studied (we have not verified this by wavelength test due to the very slow decay rates). Under this assumption, we can assess the relative rates of surface diffusion in the two systems: in POS, the transition from viscous flow to surface diffusion occurs at a much higher bulk mobility ( $\tau_{\alpha} \approx 3$  s) than in ITZ ( $\tau_{\alpha} \approx 3000$  s). Thus, surface diffusion in POS is fast enough to be the decay mechanism when bulk mobility is relatively high, but this does not happen in ITZ even at a much lower bulk mobility. From Figure 6, we estimate surface diffusion in ITZ to be  $\sim$  20 times slower than that of POS at  $\tau_{\alpha} \approx 10^7$  s (double-sided arrow).

# **Discussion**

The main result of this work is that surface diffusion is significantly slower in the glasses of the rod-like molecules POS and ITZ than in the previously studied systems (Figure 4). Between POS and ITZ, surface diffusion is slower in ITZ (Figure 6). We now discuss these results and suggest that the slow surface diffusion is a consequence of the deep penetration of the nearly vertically orientated surface molecules. We also use the new results to test a previously reported relation between surface mobility and bulk liquid fragility.

In Figure 7, we illustrate the essential difference between the surface structures of liquids composed of quasi-spherical molecules and rod-like molecules (POS and ITZ). For a liquid of quasi-spherical molecules, each surface molecule penetrates into the bulk by approximately its diameter  $d \approx \Omega^{1/3}$ , where  $\Omega$  is the molecular volume. In the case of POS, Bishop et al. have shown by NEXAFS that the rod-like molecules tend to be vertically aligned with  $\theta_z \approx 33^\circ$ , where  $\theta_z$  is the average angle between the long axis of the molecule  $n_L$  and the surface normal  $n_z$ . (For

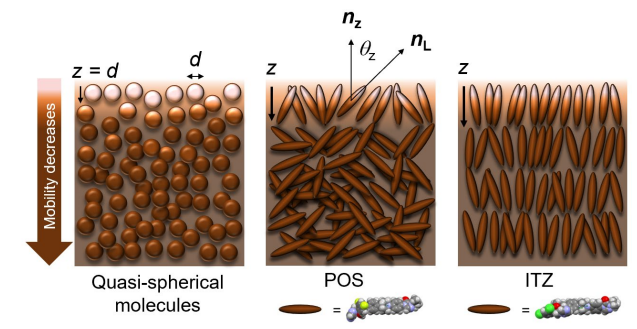


**Figure 7.** Different surface molecular structures of liquids of quasi-spherical molecules and rod-like molecules POS and ITZ. While both rod-shaped, ITZ molecules form a smectic LC phase whereas POS molecules produce an isotropic liquid. For quasi-spherical molecules, the depth of penetration of a surface molecule is approximately its diameter, z = d. The depth of penetration can be significantly larger for vertically oriented rod-like molecules. This anchors them deeper in the bulk where mobility is low, hindering their center-of-mass diffusion.

this discussion, we take each rod-like molecule as centrosymmetric and  $\theta_z$  to be positive.) Preferred

orientation at interfaces has been observed for many non-spherical molecules and is a result of free-energy minimization in an environment lacking translational symmetry. <sup>36, 37, 38</sup> We estimate the depth of penetration for a surface molecule as  $z = L \cos \theta_z$ , where  $L \approx 2.6$  nm is the length of a POS molecule in its crystals. <sup>27</sup> This yields a penetration depth of 2.2 nm, more than twice the value for a spherical molecule of the same volume (d = 0.97 nm), a direct result of preferred orientation.

254255

256

257

258

259

260

261

262

263

264

265

266

267

268

269

270

271

272

273

274

275

250

251

252

253

In the case of ITZ, the bulk liquid is a smectic LC in the temperature range of our study, and this can influence the orientational order of surface molecules. In the bulk smectic phase, rod-like ITZ molecules tend to be parallel with the LC director forming an average angle of 27°. 18 At the vapor interface, the LC director favors a vertical orientation (homeotropic alignment); this is seen from the annealing behavior of a vapor-deposited glass film.<sup>39</sup> The surface anchoring effect has been observed with other rod-like, LC-forming molecules. 40 Furthermore, simulations have shown that surface molecules of a LC can be slightly more vertically aligned than in the bulk. 41 Together, these results indicate that ITZ molecules favor a vertical orientation at the free surface and that their orientational order should be higher than that of POS molecules. From its bulk orientational order and its length of 2.8 nm (in crystals), 42 we estimate the depth of penetration for an ITZ surface molecule to be 2.5 nm.

277

278

279

280

276

Our central hypothesis is that the diffusion rate of surface molecules is determined by their depth of penetration into the bulk. Because mobility

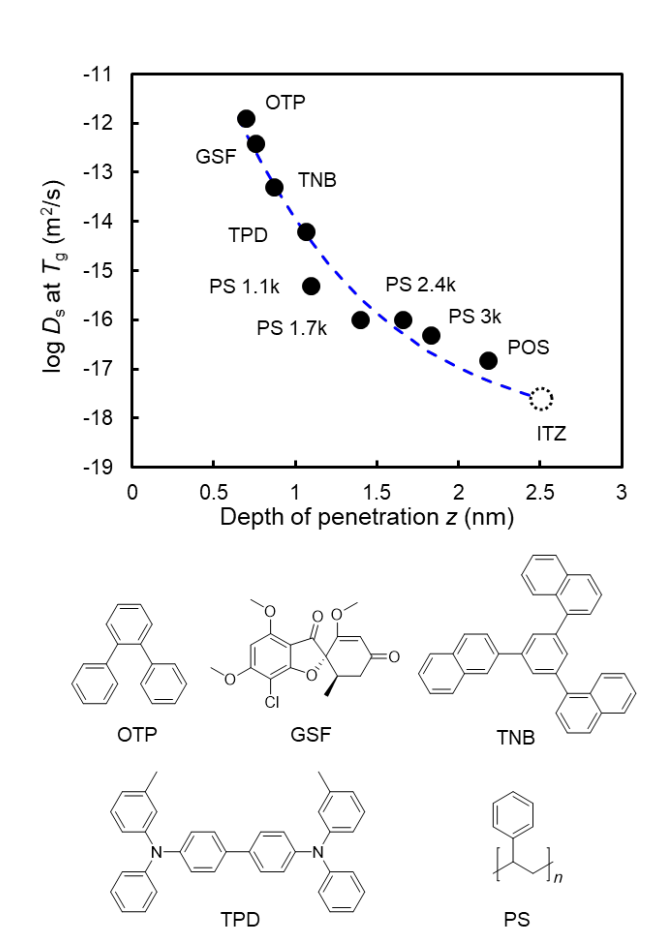


**Figure 8.** Surface diffusion coefficient  $D_s$  at  $T_g$  as a function of the penetration depth z. For quasispherical molecules OTP, GSF, and TNB,  $z \approx d$  (mean molecular size). For rod-like molecules TPD, POS, and ITZ,  $z = L \cos \theta_z$ , where L is the length of the molecule and  $\theta_z$  is the average angle between the molecular long axis and the surface normal. For chain-like PS oligomers,  $z = R_{ee} \cos \theta_{zec}$ , where  $R_{ee}$  is the end-to-end distance and  $\theta_{zec}$  the average angle between the  $R_{ee}$  vector and the surface normal. The curve is a fit of the experimental data using a double-exponential form (eq. (2)) thought to represent the surface mobility gradient of a molecular glass. The arrow indicates the estimated  $D_s$  for ITZ based on extrapolation of the fitting curve.

decreases rapidly across a vapor/glass interface, we expect the translational mobility of a surface molecule to be limited by its bottom part where mobility is the lowest, even if its top part is in a region of higher mobility. We test this idea in Figure 8 by plotting the surface diffusion coefficient at  $T_{\rm g}$  as a function of the penetration depth of surface molecules, using data from this work and the literature. The molecular structures of the systems included are shown at the bottom of Figure 8 and in Scheme 1; Table 1 contains the numerical values. In this analysis, we regard OTP, GSF, and TNB as quasi-spherical molecules and use the mean molecular size  $d = \Omega^{1/3}$  to represent the depth of penetration. For the mildly elongated TPD, penetration depth is estimated in the same way as POS and ITZ:  $z = L \cos \theta_c$ , where  $L \approx 1.7$  nm and  $\theta_t \approx 51^{\circ}$  is obtained by atomistic MD simulations.<sup>48</sup> This yields z = 1.1 nm, slightly larger than the mean molecular size (d = 0.9 nm). For chain-like PS oligomers, penetration depth is calculated from  $z = R_{\rm ec} \cos \theta_c$ , where  $R_{\rm ce}$  is the end-to-end distance <sup>43</sup> and  $\theta_t$  the average angle between the  $R_{\rm ce}$  vector and the surface normal.<sup>50</sup> Given that hydrogen bonds have an independent effect on surface diffusion from molecular dimensions,<sup>3</sup> Figure 8 only includes systems without extensive hydrogen bonds. Though hydrogen bonds might be present in a POS liquid, their contribution to the total vaporization energy is negligible ( $\sim 5\%$ , based on a group-additivity calculation<sup>3,44</sup>) and we include this system in the analysis.

**Table 1.** Surface diffusion coefficients  $D_s$  of molecular glasses and other properties.

	Т <sub>е</sub> (К)	M (g/mol)	$\rho$ (g/cm <sup>3</sup> )	d (nm)	L or Ree (nm)	$S_{\rm z}$	$\theta_z$ (deg.)	z (nm)	$\log D_{\mathrm{s}}$ at $T_{\mathrm{g}}$ (m <sup>2</sup> /s)
OTP	246	230.3	1.1245	0.70	_	_	_	0.70a	-11.9 <sup>28</sup>
GSF	361	352.8	$1.35^{46}$	0.76	_	_	_	$0.76^{a}$	$-12.4^{30}$
TNB	347	456.6	$1.15^{47}$	0.87	_	_	_	$0.87^{a}$	$-13.3^{29}$
TPD	330	516.7	$1.19^{2}$	0.90	$1.7^{48}$	$0.1^{48}$	51	1.1	$-14.2^{2}$
PS1100	307	990	$1.03^{49}$	1.17	$2.1^{43}$	$-0.1^{50}$	58	1.1	$-15.3^{31}$
PS1700	319	1600	$1.03^{49}$	1.37	$2.6^{43}$	$-0.1^{50}$	58	1.4	$-16.0^{31}$
PS2400	337	2264	$1.03^{49}$	1.54	$3.1^{43}$	$-0.1^{50}$	58	1.7	$-16.0^{13}$
PS3000	343	2752	$1.03^{49}$	1.64	$3.5^{43}$	$-0.1^{50}$	58	1.8	-16.311
POS	331	700.8	$1.27^{b}$	0.97	$2.6^{27}$	_	$33^{26}$	2.2	-16.8
ITZ	328	705.6	$1.27^{25}$	0.97	$2.8^{42}$	0.7°	2718	2.5	$(-17.8)^{d}$

<sup>&</sup>lt;sup>a</sup> The penetration depth of these quasi-spherical molecules are assumed to be the same as their mean molecular size, z = d.

<sup>&</sup>lt;sup>b</sup> Assumed to be the same as that of ITZ.

<sup>&</sup>lt;sup>c</sup> Calculated from the  $S_z$  value from Ref. 18 (bulk value).

<sup>&</sup>lt;sup>d</sup> Estimated based on trends in Figures 8 and 9.

Based on our hypothesis, we expect the rate of surface diffusion to decrease with the depth of penetration. This is indeed observed in Figure 8. We see a smooth falling trend starting from the three quasi-spherical molecules (OTP, GSF, and TNB), to the mildly elongated TPD, to the chain-like PS oligomers, and finally to the rod-like POS. These systems cover a 5 orders of magnitude in  $D_s$  and a penetration depth from 0.7 nm (OTP) to 2.2 nm (POS). The open circle indicates the estimated  $D_s$  for ITZ by extrapolation (see below).

The smooth trend observed in Figure 8 suggests that the molecular glasses considered have a similar mobility vs depth profile when compared at  $T_g$  and that the different surface diffusion rates simply reflect the different depths at which surface molecules are anchored. In principle, each system in Figure 8 has its own mobility vs depth profile. But given the smooth trend observed, a reasonable first approximation is to treat it as a generic mobility profile for van der Waals molecular glasses at  $T_g$ . One support for this notion is that the profile in Figure 8 is in rough agreement with the prediction of Mirigian and Schweizer. For disjointed Kuhn monomers of polystyrene, they predict a mobility profile of similar shape where the first nanometer of penetration leads to a 6-decade loss of mobility; they regard the profile as representative of molecular glasses like OTP and TNB. Furthermore, the trend in Figure 8 is consistent with the "double-exponential" form for surface mobility gradient observed in simulations:  $^{20,21}$ 

320 
$$\tau(z) = \tau_{\alpha} \exp[-A \exp(-z/\xi)]$$
 (2)

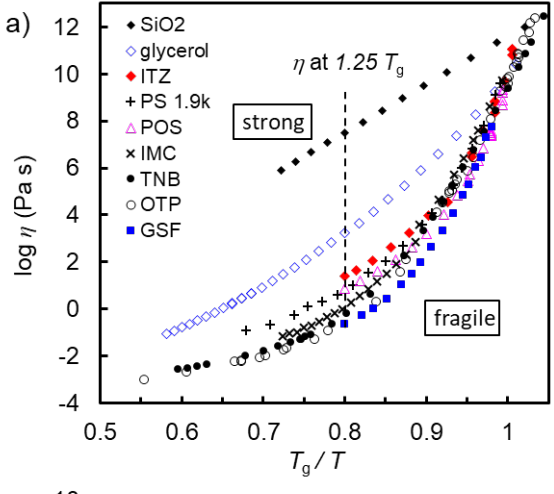
where  $\tau_{\alpha}$  is the bulk relaxation time, A is a "surface-enhancement" factor, and  $\xi$  is the dynamical correlation length. This form is thought to arise from an activation barrier for local relaxation that increases exponentially with depth. Phan and Schweitzer have rationalized this as a consequence of geometric-like, layer-wise transfer of caging constraint from the surface to the bulk. 51,52 The curve in Figure 8 is a fit of the data to eq. (2). In this fitting, we assume  $\tau_{\alpha} = 10$  s at  $T_{\rm g}$  and estimate  $\tau(z)$  from the equation:  $D_{\rm s}(z) = d^{2}/[4\tau(z)]$ . In essence, the last equation assumes the observed  $D_{\rm s}$  is determined by the local mobility at the depth of penetration z. Figure 8 shows that eq. (2) can accurately describe the experimental data. This argues that despite their different chemistry, the molecular glasses considered have a similar mobility profile  $\tau(z)$  at  $T_{\rm g}$ . From this fitting, we obtain  $\xi = 1$  nm, consistent with the values obtained from simulations.  $^{20,21}$ 

We now turn to the slower surface diffusion of ITZ relative to POS. Based on the ideas developed above, the simplest explanation is that the deeper penetration of ITZ surface molecules (2.5 nm vs 2.2 nm) anchor them deeper in the bulk where mobility is lower. This leads to slower center-of-mass diffusion. In Figure 8, we extrapolate the double-exponential fit of the experimental data points to the penetration depth of ITZ to estimate its surface diffusion rate. This yields  $\log D_s$  (m<sup>2</sup>/s) = -17.6 at  $T_g$ , in agreement with our finding that surface diffusion is slower in ITZ than in POS (Figure 6).

Chen et al. have performed a similar analysis to that presented in Figure 8 using the mean molecular size d to represent the penetration depth.<sup>3</sup> Their  $D_s$  vs d plot includes all the systems in Figure 8 except for POS and ITZ. Their plot shows a smooth decreasing trend, but when included in their plot, the rod-like molecules are outliers. For example, the  $D_s$  of POS is 30 times smaller than that of PS1110, but the two molecules have similar d values (Table 1). This is because d can represent the penetration depth of quasi-spherical molecules but not rod-shaped molecules like POS. Because of its near vertical orientation, POS penetrates deeper into the bulk than a spherical molecule of the same volume. It is interesting to note that for the chain-like PS oligomers, d is not greatly different from the estimated depth of penetration z (Table 1). This is because the  $R_{ee}$  vector of PS tends toward a parallel orientation at the surface, <sup>50</sup> reducing the depth of penetration.

Correlation between Surface Diffusion and Bulk Fragility. Chen et al. 53 reported a correlation between

the rate of surface diffusion and the fragility of the bulk liquid, with stronger liquids having slower surface diffusion when compared at  $T_{\rm g}$ . This correlation is useful for predicting surface mobility from the dynamics of bulk liquids. In Figure 9, we test this correlation using the data from this work and the recently reported data on GSF.<sup>30</sup> We plot the D<sub>s</sub> value at  $T_g$  against the viscosity of the bulk liquid at 1.25  $T_g$ (Figure 9a), used as a measure of fragility.<sup>53</sup> While the m index (slope of each curve in Figure 9a taken at  $T_g$ ) is often used to measure fragility, it is sensitive to errors of slope-taking in a temperature region where viscosity varies rapidly. 54 Our choice has the advantage of comparing experimental viscosity at a temperature at which displacement from the Arrhenius behavior is large. For GSF, the viscosity data are from Ref. 55, with a small extrapolation to high temperature through a VFT fit (Figure S1). For POS and ITZ, the literature viscosity is extrapolated with the aid of  $\tau_{\alpha}$ assuming the two have the same temperature dependence (Figures S2 and Figure S3).<sup>19</sup> Figure 9b shows that the new data points for GSF and POS both fall on the trend of the previous data, confirming the conclusion that stronger liquids have slower surface



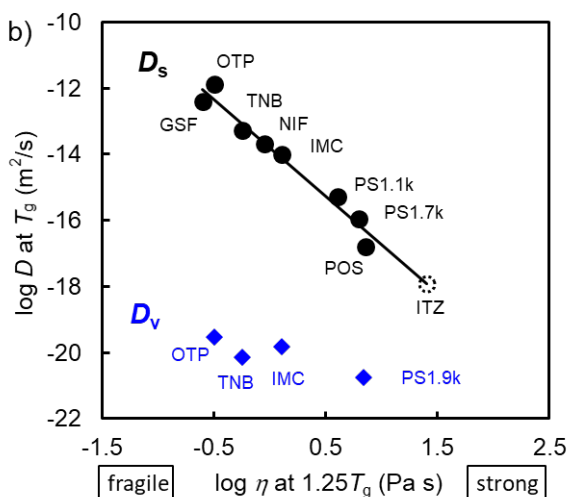


**Figure 9.** (a) Angell plot of viscosity of glass-forming liquids as a function of temperature scaled by DSC  $T_{\rm g}$ . Viscosity at 1.25  $T_{\rm g}$  is used as a measure of fragility. (b) Correlation between diffusion coefficients and bulk liquid fragility. The ITZ point (open circle) is estimated by extrapolating the trend for the other data points to the viscosity of ITZ at 1.25  $T_{\rm g}$ .

diffusion. In contrast to the strong dependence of  $D_s$  on fragility, the bulk diffusion coefficient  $D_v$  has a much weaker dependence (if at all). The surface diffusion coefficient of ITZ can be estimated by extrapolating the trend to the viscosity of ITZ at1.25  $T_g$ . This yields  $\log D_s$  (m<sup>2</sup>/s) = -17.9, in good agreement with the estimate in Figure 8,  $\log D_s$  (m<sup>2</sup>/s) = -17.6, using the penetration depth of ITZ molecules. The average of these two values is entered in Table 1 as a preliminary result for ITZ.

350

351

352

353

354

355

356

357

358

359

360

361

362

363

364

365

366

367

368

369

370

371

372

373

374

375

376

377

378

According to Chen et al.,<sup>53</sup> the correlation in Figure 9 is interpreted as follows. Fragility measures how easily a liquid's dynamics is excited when temperature is raised above  $T_g$ ; strong liquids resist this excitation, while fragile liquids is excited easily. The change of molecular environment from the bulk to the surface can also be regarded as a form of excitation (loss of nearest neighbors and decrease of density) and a stronger liquid might be expected to resist this excitation more than a fragile liquid. In its application to polymer melts, the elastically collective nonlinear Langevin equation (ECNLE) theory makes a connection between fragility and the relative importance of cage constraint and elastic penalty in segmental rearrangement and associates high fragility with dominance by elastic penalty. <sup>56</sup> Application of the theory to surface dynamics could provide a quantitative understanding of the observed correlation in Figure 9.

#### Conclusion

In summary, the method of surface grating decay has been used to measure surface diffusion in the glasses of two rod-like molecules POS and ITZ. Despite their similarity, the two systems differ in that ITZ forms liquid-crystalline phases while POS does not. We find that surface diffusion in these systems is significantly slower than in the glasses of quasi-spherical molecules of similar volume when compared at  $T_{\rm g}$ . This is attributed to the near-vertical orientation of the rod-like molecules at the surface, allowing deep penetration into the bulk where mobility is low. At the same bulk mobility, ITZ has slower surface diffusion than POS. This is attributed to a deeper penetration of the ITZ surface molecules into the bulk.

We find that for van der Waals molecular glasses (without extensive hydrogen bonds), the surface diffusion rate slows down smoothly with the depth of penetration of surface molecules (Figure 8). The mobility vs depth profile is in good agreement with the double-exponential form observed by simulations and explained by the ECNLE theory. This argues for a generic surface mobility gradient for molecular glasses and the different surface diffusion rates simply reflect the different depths at which surface molecules are anchored. This picture, if valid, allows the use of surface diffusion rate as a probe for the surface mobility gradient, a topic of considerable current interest<sup>20</sup> and a challenging target for direct experimental investigations.

The smooth trend of surface diffusivity as a function of the penetration depth of surface molecules is potentially useful for predicting surface mobility (Figure 8). For quasi-spherical molecules, the penetration depth is simply the molecular size. For chain-like and rod-like molecules, the penetration depth depends on the orientation of surface molecules relative to the interface and this can be determined by experimental techniques such as NEXAFS<sup>26</sup> and SFG<sup>57</sup> and by MD simulations.<sup>48</sup> For the purpose of predicting surface mobility, another intriguing prospect is to use the correlation between the rate of surface diffusion and the fragility of the bulk liquid (Figure 9).

The surface mobility trend allows contact with recent studies of physical vapor deposition. During vapor deposition, surface mobility allows equilibration leading to formation of high stability, high density glasses. While the measure of surface mobility most relevant for vapor deposition may not be surface diffusion, Figure 8 allows the speculative conclusion that the best possible glass packing (the "ideal glass") would be most easily approached with small molecules. Indeed, recent experiments have shown that ethylbenzene and toluene can closely approach ideal glass packing when prepared by vapor deposition. 58,59,60

To our knowledge, this work is the first to study the surface diffusion of an anisotropic organic solid (the vitrified liquid crystal of ITZ). We find that surface diffusion in ITZ is slower than that in the similar but non-LC system POS. At present it is unclear whether the effect is purely a result of the deeper penetration of ITZ molecules or reflects further constraints by the bulk crystalline phase. Further work in this area will provide insight on surface mobility in crystalline solids.

# **Supporting Information**

Viscosity and structural relaxation time for GSF, POS and ITZ.

## **Conflicts of interest**

There are no conflicts of interest to declare.

## Acknowledgements

- This research was primarily supported by NSF through the University of Wisconsin Materials Research
- Science and Engineering Center (Grant DMR-1720415). We thank Paul Voyles for helpful discussions.

441

442

## References

<sup>1</sup> L. Zhu, C. W. Brian, S. F. Swallen, P. T. Straus, M. D. Ediger and L. Yu, *Phys. Rev. Lett.*, 2011, **106**, 256103.

<sup>&</sup>lt;sup>2</sup> Y. Zhang, R. Potter, W. Zhang and Z. Fakhraai, Soft Matter, 2016, 12, 9115-9120.

<sup>&</sup>lt;sup>3</sup> Y. S. Chen, Z. X. Chen, M. Tylinski, M. D. Ediger and L. Yu, *J. Chem. Phys.*, 2019, **150**, 024502.

<sup>&</sup>lt;sup>4</sup> J. D. Stevenson and P. G. Wolynes, *J. Chem. Phys.*, 2008, **129**, 234514.

<sup>&</sup>lt;sup>5</sup> S. Mirigian and K. S. Schweizer, *J. Chem. Phys.*, 2015, **143**, 244705.

<sup>&</sup>lt;sup>6</sup> Y. Sun, L. Zhu, K. L. Kearns, M.D. Ediger and L. Yu, *Proc. Natl. Acad. Sci.*, 2011, **108**, 5990.

<sup>&</sup>lt;sup>7</sup> T. Wu and L. Yu, *Pharm. Res.*, 2006, **23**, 2350.

<sup>&</sup>lt;sup>8</sup> Y. Li, J. Yu, S. Hu, Z. Chen, M. Sacchetti, C.C. Sun and L. Yu, *Mol. Pharm.*, 2019, **16**, 1305.

<sup>&</sup>lt;sup>9</sup> S. F. Swallen, K. L. Kearns, M. K. Mapes, Y. S. Kim, R. J. McMahon, M. D. Ediger, T. Wu, L. Yu and S. Satija, *Science*, 2007, **315**, 353.

<sup>&</sup>lt;sup>10</sup> L. Berthier, P. Charbonneau, E. Flenner and F. Zamponi, *Phys. Rev. Lett.*, 2017, **119**, 188002.

<sup>&</sup>lt;sup>11</sup> Y. Chai, T. Salez, J. D. McGraw, M. Benzaquen, K. Dalnoki-Veress, E. Raphaël and J. A. Forrest, *Science*, 2014, **343**, 994-999.

<sup>&</sup>lt;sup>12</sup> Z. Fakhraai and J. A. Forrest, *Science*, 2008, **319**, 600-604.

<sup>&</sup>lt;sup>13</sup> Z. Yang, Y. Fujii, F. K. Lee, C. H. Lam and O. K. Tsui, *Science*, 2010, **328**, 1676-1679.

<sup>&</sup>lt;sup>14</sup> P. E. Acosta-Alba, O. Kononchuk, C. Gourdel and A. Claverie, J. Appl. Phys., 2014, 115, 134903.

<sup>&</sup>lt;sup>15</sup> M. D. Ediger, J. J. de Pablo and L. Yu, *Acc. Chem. Res.*, 2019, **52**, 407.

<sup>&</sup>lt;sup>16</sup> E. J. Rachwalski, J. T. Wieczorkiewicz and M. H.Scheetz, Ann. Pharm., 2008. 42, 1429.

<sup>&</sup>lt;sup>17</sup> M. Boogaerts, D. J. Winston, E. J. Bow, G. Garber, A. C. Reboli, A. P. Schwarer, N. Novitzky, A. Boehme, E. Chwetzoff and K. De Beule, *Annals of internal medicine*, 2001, **135**, 412.

<sup>&</sup>lt;sup>18</sup> M. Tarnacka, K. Adrjanowicz, E. Kaminska, K. Kaminski, K. Grzbowska, K. Kolodziejczyk, P. Wlodarczyk, L. Hawelek, G. Garbacz, A. Kocot and M. Paluch, *Phys. Chem. Chem. Phys.*, 2013, **15**, 20742.

<sup>&</sup>lt;sup>19</sup> K. Adrjanowicz, K. Kaminski, P. Wlodarczyk, K. Grzybowska, M. Tarnacka, D. Zakowiecki, G. Garbacz, M. Paluch and S. Jurga, *Mole. Pharm.*, 2013, **10**, 3934.

<sup>&</sup>lt;sup>20</sup> P. Scheidler, W. Kob and K. Binder, *Europhys. Lett.*, 2002, **59**, 701

<sup>&</sup>lt;sup>21</sup> K. S. Schweizer and D. S. Simmons, *J. Chem. Phys.*, 2019, **151**, 240901.

<sup>&</sup>lt;sup>22</sup> W.W. Mullins, *J. Appl. Phys.*, 1959, **30**, 77.

<sup>&</sup>lt;sup>23</sup> P. S. Maiya and J. M. Blakely, *J. Appl. Phys.*, 1967, **38**, 698-704.

<sup>&</sup>lt;sup>24</sup> R. Malshe, M. D. Ediger, L. Yu and J. J. de Pablo, *J. Chem. Phys.*, 2011, **134**, 194704.

<sup>&</sup>lt;sup>25</sup> K. Six, G. Verreck, J. Peeters, M. Brewster and G. V. D. Mooter, J. Pharm. Sci., 2004, 93, 124

<sup>&</sup>lt;sup>26</sup> C. Bishop, J. L. Thelen, E. Gann, M. F. Toney, L. Yu, D. M. DeLongchamp and M. D. Ediger, *Proc. Natl. Acad. Sci.*, 2019, **116**, 21421.

<sup>&</sup>lt;sup>27</sup> D. K. McQuiston, M. R. Mucalo and G. C. Saunders, *J. Mol. Struc.*, 2019, **1179**, 477.

<sup>&</sup>lt;sup>28</sup> W. Zhang, C. W. Brian and L. Yu, *J. Phys. Chem. B.*, 2015, **119**, 5071.

<sup>&</sup>lt;sup>29</sup> S. Ruan, W. Zhang, Y. Sun, M. D. Ediger and L. Yu, *J. Chem. Phys.* 2016, **145**, 064503.

<sup>&</sup>lt;sup>30</sup> C. Huang, S. Ruan, T. Cai and L. Yu, *J. Phys. Chem.* B., 2017, **121**, 9463.

<sup>&</sup>lt;sup>31</sup> W. Zhang and L. Yu, *Macromolecules.*, 2016, **49**, 731.

<sup>&</sup>lt;sup>32</sup> M. K. Mapes, S. F. Swallen and M. D. Ediger, *J. Phys. Chem. B.*, 2006, **110**, 507.

<sup>&</sup>lt;sup>33</sup> S. F. Swallen, K. Traynor, R. J. McMahon, M. D. Ediger and T. E. Mates, *J. Phys. Chem. B.*, 2009, **113**, 4600.

<sup>&</sup>lt;sup>34</sup> S. F. Swallen, and M. D. Ediger, *Soft Matter*, 2011, **7**, 10339.

<sup>&</sup>lt;sup>35</sup> O. Urakawa, S. F. Swallen, M. D. Ediger and E. D. von Meerwall, *Macromolecules*, 2004, **37**, 1558.

<sup>&</sup>lt;sup>36</sup> H. Kimura and H. Nakano, *J. Phys. Soc. Japan*, 1985, **54**, 1730.

- <sup>37</sup> A. Haji-Akbari and P. G. Debenedetti, *J. Chem. Phys.*, 2015, **143**, 214501
- <sup>38</sup> M. Sadati, H. Ramezani-Dakhel, W. Bu, E. Sevgen, Z. Liang, C. Erol, M. Rahimi, N. Taheri Qazvini, B. Lin, N. Abbott, B. Roux, M. Schlossman and J. de Pablo, *J. Amer. Chem. Soc.*, 2017.**139**, 3841.
- <sup>39</sup> C. Bishop, A. Gujral, M. F. Toney, L. Yu and M. D. Ediger, *J. Phys. Chem. Lett.*, 2019, 10, 3536.
- <sup>40</sup> B. Jerome, *Rep. Pro. Phys.*, 1991, **54**, 391.
- <sup>41</sup>M. F. Palermo, L. Muccioli and C. Zannoni, *Phys. Chem. Chem. Phys.*, 2015, **17**, 26149.
- <sup>42</sup> M. Lahtinen, E. Kolehmainen, J. Haarala and A. Shevchenko, *Crys. Growth Des.*, 2013, **13**, 346. See the CSD (C. R. Groom, I. J. Bruno, M. P. Lightfoot and S. C. Ward, *Acta Cryst.*, 2016, **B72**, 171.) for a complete list of known ITZ crystal structures, including polymorphs (code TEHZIP and code TEHZIP03) and solvates (code REWTUK). In all known ITZ crystal structures, the rod-like molecule is approximately 2.8 nm long, indicating the robustness of this value.
- <sup>43</sup> L. J. Fetters, D. J. Lohse, D. Richter, T. A. Witten and A. Zirkel, *Macromolecules*, 1994, **27**, 4639.
- <sup>44</sup> J. S. Chickos and W. E. Acree, *J. Phys. Chem. Ref. Data*, 2003, **32**, 519
- <sup>45</sup> M. Naoki and S. Koeda, *J. Phys. Chem.*, 1989, **93**, 948.
- <sup>46</sup> L. Zhu, J. Jona, K. Nagapudi and T. Wu, *Pharm. Res.*, 2010, **27**, 1558.
- <sup>47</sup> D. J. Plazek and J. H. Magill, *J. Chem. Phys.*, 1966, **45**, 3038.
- <sup>48</sup> I. Lyubimov, L. Antony, D. M. Walters, D. Rodney, M. D. Ediger and J. J. de Pablo, *J. Chem. Phys.*, 2015, **143**, 094502.
- <sup>49</sup> S. L. Simon, J. W. Sobieski and D. J. Plazek, *Polymer*, 2001, **42**, 2555.
- <sup>50</sup> A. N. Rissanou and V. Harmandaris, *Macromolecules*, 2015, **48**, 2761.
- <sup>51</sup> A.D. Phan, K.S. Schweizer, *J. Chem. Phys.*, 2019, **150**, 044508.
- <sup>52</sup> A.D. Phan, K.S. Schweizer, *Macromolecules*, 2019, **52**, 5192.
- <sup>53</sup> Y. Chen, W. Zhang and L. Yu, *J. Phys. Chem. B.*, 2016, **120**, 8007.
- <sup>54</sup> R. Richert and C. A. Angell, *J. Chem. Phys.* 1998, **108**, 9016.
- <sup>55</sup> Q. Shi, J. Tao, J. Zhang, Y. Su, T. Cai, *Crys. Growth Des.*, 2019, **20**, 24.
- <sup>56</sup> S.J. Xie, K.S. Schweizer, *Macromolecules*, 2016, **49**, 9655.
- <sup>57</sup> H. K. Nienhuys and M. Bonn, *J. Phys. Chem. B.,* **2009**, **113**, 7564.
- <sup>58</sup> M. S. Beasley, C. Bishop, B. J. Kasting and M. D. Ediger, *J. Phys. Chem. Lett.* 2019, **10**, 4069.
- <sup>59</sup> E. Leon-Gutierrez, A. Sepúlveda, G. Garcia, M. T. Clavaguera-Mora and J. Rodríguez-Viejo, *Phys. Chem. Chem. Phys.* 2016, **18**, 8244.
- <sup>60</sup> M. D. Ediger, *J. Chem. Phys.* 2017, **147**, 210901.